Absorption and refraction spectroscopy of a tunable-electron-density quantum-well and reservoir structure

M. Wegener, J. E. Zucker, T. Y. Chang, N. J. Sauer, K. L. Jones, and D. S. Chemla
AT&T Bell Laboratories, Holmdel, New Jersey 07733
(Received 28 July 1989)

We present differential absorption and refraction spectroscopy of a novel $In_xGa_{1-x}As/In_{1-y}Al_yAs$ multiple-quantum-well heterostructure in which the electron density inside the well is controlled electrically. This is achieved by providing a reservoir of electrons close to each quantum well in every fundamental building block. By applying a bias to the structure, electrons can be transferred from this reservoir into the nearby quantum well where they quench the absorption due to the Pauli exclusion principle. Our electroabsorption spectra reveal information about the Fermi energies in the quantum well and the reservoir as well as the electric fields in the well and the barrier material. In addition, we find that quenching of the quantum-well absorption is accompanied by a large change in refractive index below the quantum-well absorption edge, which is proportional to the number of electrons in the well. We demonstrate on a set of samples that the structure can be quantum mechanically engineered.

I. INTRODUCTION

The ability to modify semiconductor quantum-well (QW) optical properties by addition or removal of free carriers is of tremendous fundamental as well as technological importance.[1] Accurate control of the electron or hole density by an external bias allows studies of many-body, phase-space-filling, and electrostatic effects on the absorption spectrum, and provides a basis for optoelectronic devices utilizing carrier-induced absorption and refraction.[1] Current injection is a simple but problematic method of introducing free carriers, since the carrier density and carrier temperature are not well-defined quantities. In addition, current flow causes undesirable heating and losses. Modulation doping[2] has proven to be a powerful method of introducing permanent, thermalized electron or hole populations into the QW, which are spatially separated from the doping impurity atoms. This avoids ionized-impurity scattering. However, it does not allow a tunable density. A modulation-doped field-effect transistor (FET) has previously been employed in reflectivity studies of band filling in a single QW,[3-6] but the close proximity of the gate electrode to the well precludes normal-incidence transmission measurements and has unacceptable losses for waveguide applications. Moreover, the gate cannot accurately control the density in more than a single QW.

In this paper we present the optical and electrical characteristics of a novel structure in which any number of QW's can be stacked, each experiencing an equal voltage drop and change in electron density with applied bias. We use absorption and refraction spectroscopy to identify the important physical processes which take place in the QW and other regions of the structure.

II. STRUCTURE AND PRINCIPLE OF OPERATION

In order to study the effects of electrons on the QW absorption, it is desirable to have a sample structure that is thermodynamically closed (in terms of the carriers) such that the electron density and electron temperature in the well are well-defined quantities. This cannot be achieved in carrier-injection devices which represent a thermodynamically open system. To realize the proper closed system, we need to provide a reservoir of charges for the QW as well as an isolating barrier to suppress current flow. The In-Ga-As/In-Ga-Al-As/In-Al-As material system is particularly well suited for this type of structure. First, modulation doping is extremely effective in producing high carrier densities and mobilities in the low-band-gap $In_xGa_{1-x}As$ QW's.[7] Second, the large conduction-band discontinuity between $In_xGa_{1-x}As$ and $In_{1-y}Al_yAs$ provides a high potential barrier for electrons. Finally, the compositional flexibility of In-Ga-Al-As allows us to grade the desired potential profile around the well, reservoir, and barrier regions.

These features are illustrated in Fig. 1, which shows the central building block of the device. This block, repeated five times, forms the active core of an *n-i-n* In-Al-As/In-Ga-Al-As waveguide heterostructure. Bottom and top are contacted by Ohmic metal contacts.

× 5	120 Å	In-Ga-Al-As
	150 Å	In-Al-As
	150 Å	In-Al-As: Be $1.2\times10^{18}cm^{-3}$
	250 Å	In-Al-As
	90 Å	In-Ga-As QW
	260 Å	In-Ga-Al-As
	500 Å	In-Ga-Al-As: Si $9.8\times10^{17}cm^{-3}$

FIG. 1. Fundamental period of the novel device that has been repeated five times and forms the core of a waveguide. The cladding is provided by alternating layers of In-Ga-Al-As and In-Al-As that are *n*-type doped. The substrate is InP.

Each fundamental building block consists of the following layers. A 500-Å n-type doped In-Ga-Al-As layer provides the reservoir of electrons. It is isolated from the 90-Å In-Ga-As QW (the region to be filled) by an undoped In-Ga-Al-As spacer layer that ensures that the QW is free of impurities. The third constituent finally is the 550-Å In-Al-As region that is p-type doped in its middle. 120 Å of undoped In-Ga-Al-As make the transition to the next building block. The entire structure is grown lattice matched to InP substrate by molecular-beam epitaxy using one In cell, two Ga cells, and two Al cells.

The operation of the device can be understood in terms of the band diagram shown in Figs. 2 and 3(a)–3(c). We analytically solve Poisson's equation in the abrupt-depletion-layer approximation. To obtain this analytical result, we neglect the carriers in the QW, which is exact as long as the quantum well is empty. The quasi-Fermi-energies of electrons (E_F^e) and of holes (E_F^h) are then calculated from

$$\text{const} = j_e + j_h = N_e \mu_e \nabla(E_F^e) + N_h \mu_h \nabla(E_F^h) , \qquad (1)$$

where μ_e and μ_h are the electron and hole mobilities and N_e and N_h are the electron and hole densities. Because of the dominance of n-type doped regions, j_e = const holds. To numerically solve this nonlinear equation, one needs a relation between the electron (hole) density and the quasi-Fermi-energies. The calculation is much simplified in the Boltzmann approximation. This qualitatively gives the proper dependence, but slightly underestimates the position of the Fermi energy in the n-doped reservoir region. The finite amount of electrons in the reservoir could strictly be treated in a self-consistent manner, but for the purpose of this calculation we treat it as an infinite bath since the thickness of the reservoir is 5.6 times that of the QW to be filled. The parameters for the calculation (doping densities and layer thicknesses) refer to those of the sample described in Fig. 1. The masses are taken from the literature[3–5] In-Ga-As—$m_e/m_0 = 0.041$, $m_{hh}/m_0 = 0.377$, $m_{lh}/m_0 = 0.0516$; In-Al-As—$m_e/m_0 = 0.07$, $m_{hh}/m_0 = 0.58$, $m_{lh}/m_0 = 0.14$; In-Ga-Al-As (by linear interpolation)—$m_e/m_0 = 0.053$, $m_{hh}/m_0 = 0.46$, $m_{lh}/m_0 = 0.088$.

Figure 2 shows the calculated band diagram for four periods under positive bias. We find that the band diagram repeats itself after each fundamental building block, and thus any number of QW's can be stacked. Under the conditions of Fig. 2, all the QW's are filled with electrons. Knowing that the band diagram is periodic, we now study the filling of the QW and the associated electron transfer in more detail by concentrating on a single period. Figure 3(a) shows the band diagram of one period without bias (at room temerature). The QW rides on the left-hand slope of the potential hill formed by the n-i-p-i-n layer sequence. The p-type doped region is always completely depleted. The QW is clearly above the Fermi energy and is thus empty. The difference in energy between the ground state of the well and the Fermi energy (and thus the electron density in the QW at zero bias) can be quantum-mechanically engineered by sliding the QW up and down the potential slope, i.e., changing the QW position between the barriers. We present here data on two different samples (A and B) to demonstrate this band-gap–engineering possibility. Sample B differs from

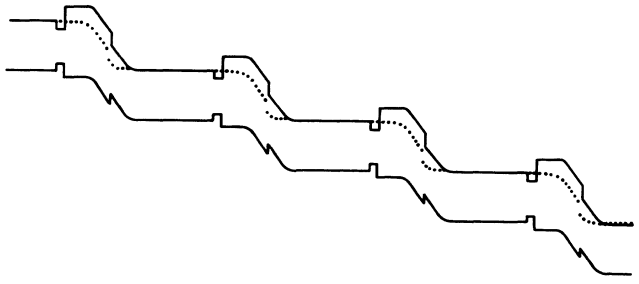

FIG. 2. Band diagram under bias for four periods of the fundamental building block.

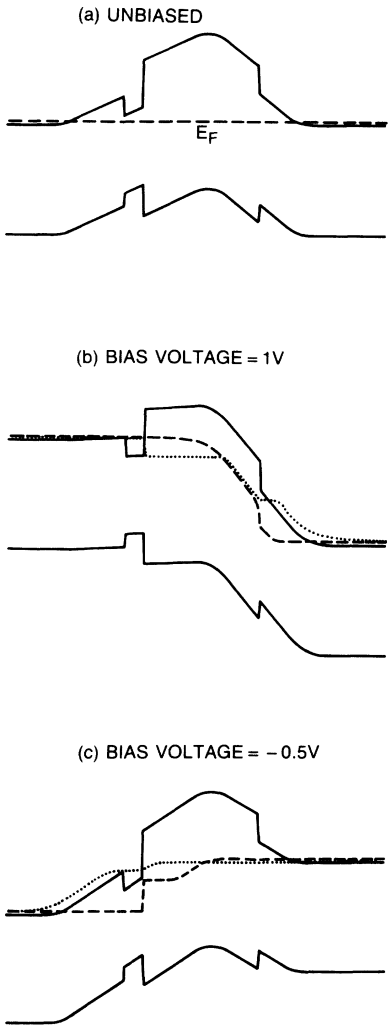

FIG. 3. Calculated band diagram of one period (a) unbiased, (b) positive voltage, and (c) negative voltage to the top of the structure. The parameters for the calculation are the actual sample parameters of sample A (see Fig. 1). Effective masses are taken from the literature.

sample A (described in Figs. 1–3) in that the QW is moved 50 Å to the left. Thus the well in sample B is closer to the Fermi energy at zero bias. Figure 3(b) shows that as a positive bias voltage is applied to the top of the structure (right-hand side of the band diagram), the right-hand side is pushed down and the QW crosses the quasi-Fermi-energy and is filled. Under this bias condition the large potential barrier in the middle is essentially reduced to the difference in the conduction-band energies between the quaternary and ternary semiconductor compounds. This energy difference determines the leakage current through the structure under bias. As shown in Fig. 3(c), if the structure is biased in the other direction, the field in the QW increases, but the QW remains empty.

Note that in the thick n-type region the flat-band condition is recovered at the end of each building block for all biases. Thus the voltage drop over each period is the same, and therefore the total voltage necessary to apply 1 V to each period is N volts. If, however, the reservoir region is not thick enough, then band bending dominates and the electron density is different in each QW.

Figure 4 shows the current-voltage characteristics for a 100-μm$\times$200-μm mesa at (a) room temperature and (b) $T=10$ K. The flow of current for positive bias is suppressed by the barrier as depicted in Fig. 3(b). Residual current is due to thermionic emission over the barrier and is eliminated with decreasing temperature. This is demonstrated in Fig. 4(b). We find that significantly higher breakdown voltages can be achieved in smaller-area devices.

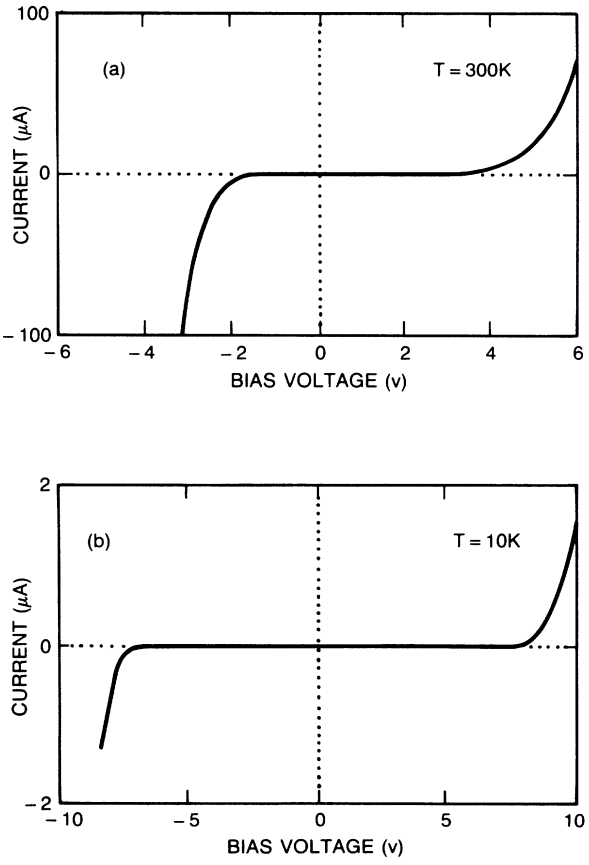

FIG. 4. Current-voltage characteristics of a 200-μm$\times$100-μm large device at (a) 300 K and (b) 10 K.

III. DIFFERENTIAL ABSORPTION SPECTROSCOPY

In normal incidence, direct absorption cannot be measured in our samples because the optical thickness of the five quantum-well structures is too small. Differential absorption spectroscopy (DAS), however, is known to be extremely sensitive since standard lock-in techniques can be applied. For the normal-incidence spectra, a tungsten lamp and a 0.25-m spectrometer are used as a light source, which gives access to a very wide spectral range. The light from the spectrometer is then imaged through the substrate onto the mesa and the transmitted light is detected with a Ge photodiode. Optical imaging from the top gives control over the alignment and the electrical probe tips that are used to make electrical contact. With integration times on the order of 1 s field-induced changes in the transmission spectrum, $\Delta T/T \approx 10^{-3}$, can easily be resolved.

Figure 5 shows three differential transmission spectra of sample A for modulation from 0 to 2, 6, and 10 V. These spectra reflect a change in the band structure from that of Fig. 3(a) to that of Fig. 3(b). The complex spectrum includes sharp features over a wide range of photon energies, indicating that several of the different band-gap materials are active in electroabsorption. In order to assign the features associated with the In-Ga-As QW, we have performed a resonant-tunneling calculation of the electron and hole energy levels of the band diagram shown in Fig. 3(a) (zero-bias condition), when the electric

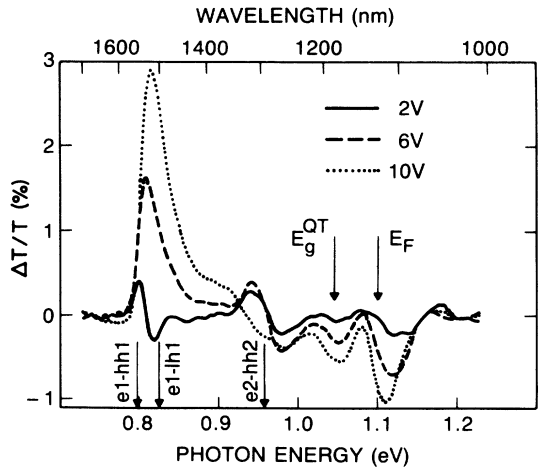

FIG. 5. Differential transmission spectra of sample A for modulation from 0 to 2, 6, and 10 V. The arrows indicate the calculated energy levels of the quantum well, the band gap of the quaternary material, and the Fermi energy in the reservoir region. The different spectral features are explained in the text.

field in the QW region is $\approx 9.4\times10^4$ V/cm. The resonant-tunneling approach is a single-particle picture in the effective-mass approximation and assumes coherence throughout the structure. Thus it neglects any kind of scattering (phonons, alloy fluctuations, etc.). The calculated values for the $e1$-hh1 and $e1$-lh1 transitions are 0.799 and 0.825 eV, respectively. The $e2$-hh2 transition is at 0.958 eV; the lh2 state is unbound. We have indicated these energies by the arrows in Fig. 5. Also shown is the band gap of the quaternary In-Ga-Al-As at 1.05 eV. The Fermi energy for the doping level of 9.8×10^{17} (cm^{-3}) in the degenerate limit is about 55 meV higher. These energies allow us to attribute the observed spectral features to the different layers of the heterostructure. At photon energies above 0.8 eV, the positive signal which increases in linewidth with increasing bias voltage is due to the occupation of the $n_z=1$ subband of the electrons as the Fermi energy crosses the lowest electronic level. Here the Pauli exclusion principle forbids absorption processes into the occupied electronic states. This simultaneously blocks the heavy- and light-hole transitions. The asymmetric line shapes centered near 0.95 eV reflect the blue shift (increased absorption at higher photon energies, decrease of absorption at lower photon energies) of the $n_z=2$ transition and are attributed to the reduction of the electric field in the QW. At higher photon energies, two features related to the quaternary In-Ga-Al-As are observed. With increasing bias, induced absorption at the quaternary band gap (1.05 eV) and around the Fermi energy in the n-type doped quaternary reservoir regions occurs. In the following we will discuss in detail the individual phenomena in each spectral region. The signal from each part of the structure yields information on Fermi energy and electric field in that region and is used to trace the path of the electron transfer. We show that, in fact, a large number of electrons can be transferred from the reservoir into the QW.

A. Processes inside the quantum well

In Fig. 6 we focus on the $n_z=1$ and $n_z=2$ transitions of the quantum well. For small positive voltages [Fig. 6(a)], both the $n_z=1$ and $n_z=2$ levels exhibit an asymmetric line shape, which indicates a blue shift, i.e., increased absorption at higher photon energies and decreased absorption at lower photon energies. This is associated with the reduction of the built-in field. Integration of the differential signal about the $n_z=1$ transition yields zero, indicating that the oscillator strength is conserved and the electron density remains zero upon application of the field. However, as progressively higher biases are applied, the asymmetric line shape is transformed into a signal which is only positive. This bleaching shows that the oscillator strength of the $n_z=1$ transition is being reduced by the presence of the electrons. The Fermi energy has crossed the lowest electronic level and thus the QW is becoming full. For increasing bias the high-energy edge of this quenched spectral region clearly blue-shifts as the number of electrons in the QW increases. For 8 V bias and above, the $n_z=1$ transition starts to merge with the electroabsorption associated with the $n_z=2$ transition.

The behavior of the $n_z=2$ transition as the voltage is increased is distinctly different from that of the $n_z=1$ transition. Since the $n_z=2$ level remains unoccupied, its signal continues to give information about the electric field in the QW even as the $n_z=1$ level is filled. Only at the highest biases does the $n_z=2$ transition line shape change, due to renormalization effects and broadening.[8] For moderate electron densities, higher-lying transitions ($n_z>1$) are not strongly influenced by carrier-induced renormalization.[8] For high electron densities, however, the renormalization becomes noticable, as shown in Fig. 6(a). We observe a negative differential signal below the $n_z=2$ transition at around 0.95 eV, where at lower biases a positive signal is apparent. This negative signal indicates increased absorption below the $n_z=2$ transition. This corresponds to a red shift (renormalization) or a broadening of this transition.

To confirm our interpretation that the electrons in the QW originate from the reservoir and are not simply injected from the contacts, we study the other bias direction. The calculated band diagram of Fig. 3(c) predicts an increased electric field in the QW region. This, conse-

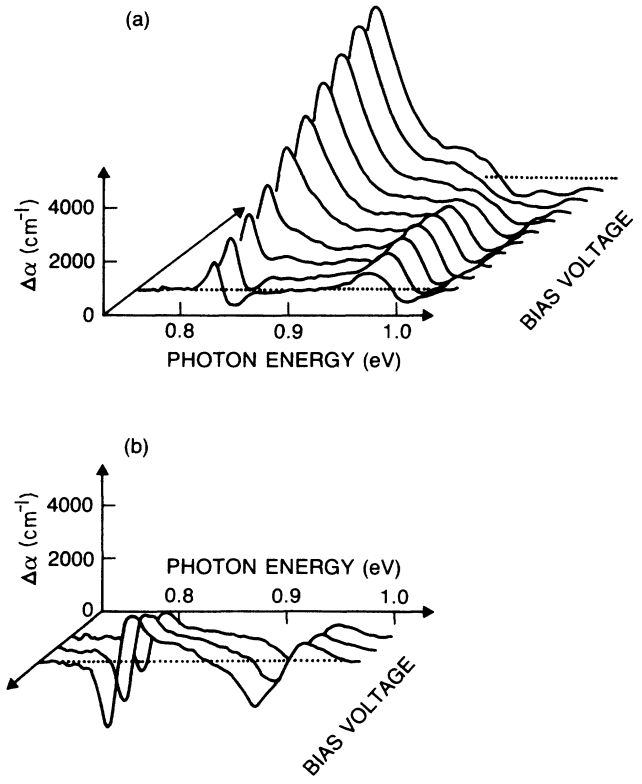

FIG. 6. Differential absorption spectra of sample A displaying the quantum-well-related features for both bias directions starting from 2 V and progressing in 1-V steps. For positive voltages a successive filling of the $n_z=1$ subband can be seen. The $n_z=2$ subband at low bias voltage represents the reduction of the built-in field with increasing bias. At higher voltages a renormalization and broadening due to the high electron density dominates the line shape. For negative bias both subbands show a differential line shape which is characteristic of the quantum confined Stark effect.

quently, should lead to the quantum confined Stark effect,[9] i.e., a red shift of the optical transitions. As can be seen from Fig. 6(b), this is, in fact, observed. The increased (decreased) absorption at lower (higher) photon energies clearly reflects this red shift, for both the $n_z=1$ and $n_z=2$ transitions. The presence of only field effects for negative bias and the symmetry of our structure rules out carrier injection for both bias directions.

1. $n_z=1$ heavy- and light-hole features

So far we have not considered the special nature of the QW valence-band structure. These features are illustrated in Fig. 7 for the particular voltage range where the Fermi energy crosses the $n_z=1$ electronic sublevel. For 3 V bias in Fig. 7(a) (sample *A*), two distinct maxima become visible. Further increase of the bias voltage (and thus of the electron density) reduces the higher-energy feature to a mere shoulder. The origin of this behavior is understood as follows. At low electron densities only the lowest electronic states are occupied. This simultaneously blocks the heavy- and light-hole transitions. Under these conditions we observe two distinct maxima. As the electron density increases, the heavy-hole transitions are quenched further and further until the spectral width of the quenched area exceeds the heavy-hole–light-hole splitting. At this point we no longer resolve two distinct maxima in the DAS, but the light-hole signal degenerates to a shoulder in the quenched heavy-hole absorption. This interpretation is confirmed by the waveguide spectra reported in Sec. III A 2.

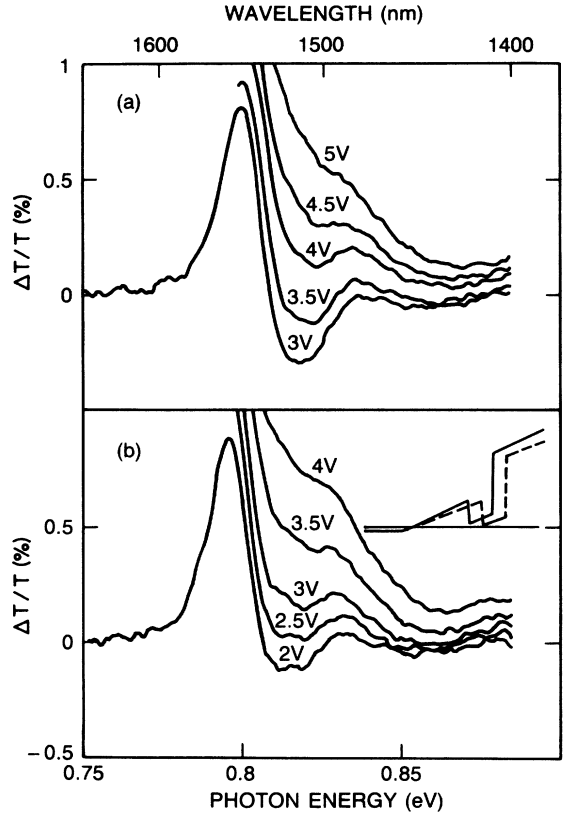

FIG. 7. Detail of the differential transmission spectra of samples (a) *A* and (b) *B* at the crossing of the Fermi energy with the lowest electron level in the quantum well. At the crossing point both the heavy and light hole can clearly be resolved. For increasing electron density the heavy-hole resonance is quenched to energies higher than the light-hole resonance. At this point the light-hole signal reduces to a shoulder on the high-energy wing of the heavy-hole bleaching. The inset shows sample *A* (dotted) unbiased and sample *B* (solid line) with 1 V bias. Clearly, 1 V bias difference compensates for the different energetic positions of the quantum wells relative to the Fermi level. This nicely demonstrates the possibility to quantum-mechanically engineer the structure.

This particular spectral feature is a signature of the crossing of the Fermi energy with the lowest electronic sublevel. As mentioned in Sec. II, we are able to quantum-mechanically engineer the band diagram by sliding the QW up or down the energetic slope created by the *n-i-p-i-n* doping sequence of the fundamental building block. In sample *B* we have moved the QW 50 Å down this slope, and thus the lowest electronic subband is about 50 meV closer to the Fermi energy. The inset of Fig. 7(b) illustrates this difference. A 1-V bias difference between the two samples compensates for the different initial separations between the QW and Fermi energy.

In Fig. 7(b) we show the crossing regime for sample *B*. As can be seen, the same qualitative behavior of the light-hole resonance is present. However, all bias voltages are shifted by approximately 1 V, which is in good agreement with the calculation of the band diagrams. By shifting the QW further down the slope or by reducing the *p*-type doping in the barrier layer, we can also achieve a condition where the QW is already filled at zero bias. Figure 7 also confirms that the calculated band diagrams give a reliable qualitative representation of the real processes.

2. Polarization-dependent waveguide spectra

In our waveguide structure the higher refractive index of the active core region relative to In-Al-As cladding layers permits propagation of the light in the plane of the QW layers. In this geometry we are able to measure electroabsorption spectra in TM polarization (optical polarization vector perpendicular to the QW layers) that is inaccessible under normal incidence, as well as in TE polarization (polarization vector in the plane of the QW). The inset of Fig. 8 illustrates the waveguide geometry and the calculated light-intensity profile of the fundamental waveguide mode. It can be seen that the five QW's (each shown to scale as a solid line) occupy only a small fraction ($\approx 10^{-2}$) of the entire optical mode. Thus the overall absorption in the waveguide is low and we are able to obtain differential absorption spectra at wavelengths both above and below the $n_z=1$ hh and lh transitions. Lateral confinement of the propagating light is achieved by etching ribs 3 μm wide. The total waveguide length is 520 μm. The optical source for the waveguide spectra is a cw neodymium-doped yttrium lithium fluoride (YLF:Nd) laser pumped NaCl-F^{2+} color-center laser which is coupled in and out of the cleaved

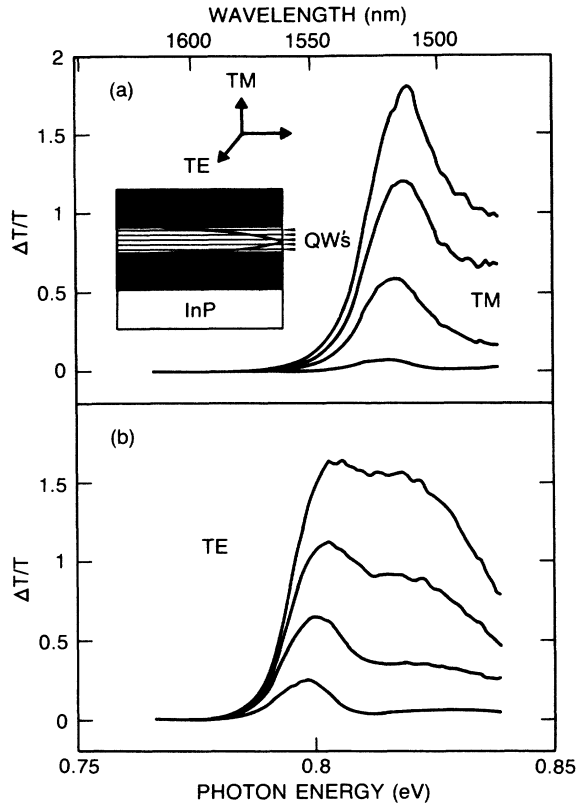

FIG. 8. Waveguide differential transmission spectra for (a) TM and (b) TE polarization of the incoming light. The inset illustrates the geometry. For TM polarization the selection rules forbid the electron–heavy-hole transition and only the light-hole resonance appears. This leads to a maximum light modulation at around 1550 nm in TE polarization, whereas in TM polarization essentially no light modulation is observed at this wavelength.

waveguide facets with microscope objectives. The light level is kept sufficiently low to avoid saturation due to light.

Figures 8(a) and 8(b) show the differential absorption spectra for (a) TE and (b) TM polarization for various bias voltages. On the high-energy side we are, unfortunately, limited by the tuning range of our laser system. The longer optical interaction length of the waveguide as compared to normal incidence clearly enhances the transmission change. Furthermore, we now can confirm our assignment of heavy- and light-hole-originated signals by studying the two different polarizations. In TM polarization only the $e1$-lh1 transition is dipole allowed. In TE polarization both heavy- and light-hole transitions appear. This definitively proves our assignment of the two maxima in the normal-incidence and the TE spectra. Note, also, that the selection rules lead to a strong polarization anisotropy: light at 0.8 eV is clearly modulated for TE polarization, but is essentially not modulated for the TM polarization.

B. Reservoir depletion

We have thus far only discussed changes in absorption associated with the QW. However, the electrons which appear in the QW according to our interpretation originate from the reservoir. To monitor this process, we can look for a small reduction in the Fermi energy of the reservoir material as electrons are moved into the QW. This is expected because the reservoir is not infinite.

In the present structure the reservoir region of each fundamental building block is 500 Å thick. The QW is 5.6 times thinner. If we, for example, transfer 10^{12} cm^{-2} electrons into the QW, thus raising the Fermi energy in the In-Ga-As QW to ≈ 50 meV above the gap, the electron density in the reservoir diminishes from 9.8×10^{17} to 7.8×10^{17} cm^{-3}. In the reservoir this corresponds to a shift of the Fermi energy from $E_F=E_g+54.4$ meV to $\tilde{E}_F=E_g+46.8$ meV; $\tilde{E}_F$ is the depleted-reservoir Fermi energy. Figure 9 focuses on this spectral region. The dominant structure in Fig. 7(a) is the induced absorption around 1100 nm, close to the Fermi energy of the reservoir material. We interpret this in terms of an effective red shift of the Fermi energy as shown in Fig. 9(b). As a positive bias is applied, electrons move from the reservoir into the QW. Thus the reservoir is depleted by a small amount. In Fig. 9(b) we plot the function

$$\alpha(h\nu)=\alpha_0(h\nu)[1-f_e(h\nu)]\ , \tag{2}$$

where $f_e(h\nu)$ is the electron Fermi function. For simpli-

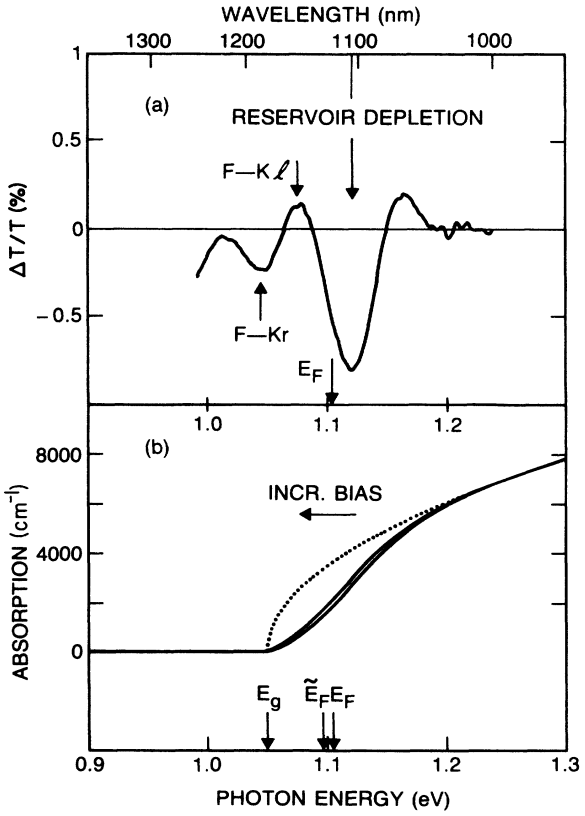

FIG. 9. (a) Experiment: detail of the signal related to the quaternary material. The most pronounced feature below the Fermi energy is due to the reduced number of electrons in the reservoir regions as electrons are transferred into the QW's. (b) Simple model calculation that confirms this interpretation.

city, we assume a bulklike square-root density of states for the absorption coefficient in the absence of electrons, $\alpha_0(h\nu)$. The difference in the calculated curves for E_F and $\tilde{E}_F$ agrees well with the measured signal in Fig. 9(a), which reflects 2500 Å of material.

In addition to the main feature, Fig. 9(a) exhibits further structure in the spectrum around the quaternary band gap, 1.05 eV. We interpret this as being due to the changing electric fields in the undoped or depleted quaternary regions. The electric field on the left (right) decreases (increases) as positive bias is applied. [See Figs. 3(a) and 3(b).] The associated Franz-Keldysh effect thus leads to induced absorption below the respective gap on the left-hand side (arrow FK *l*) and induced absorption below the respective gap on the right-hand side (arrow FK *r*).

The observation of the reservoir signal and our quantitative interpretation of it proves that electrons are, in fact, effectively transferred from the reservoir into the QW. The total number of electrons in each fundamental building block is conserved.

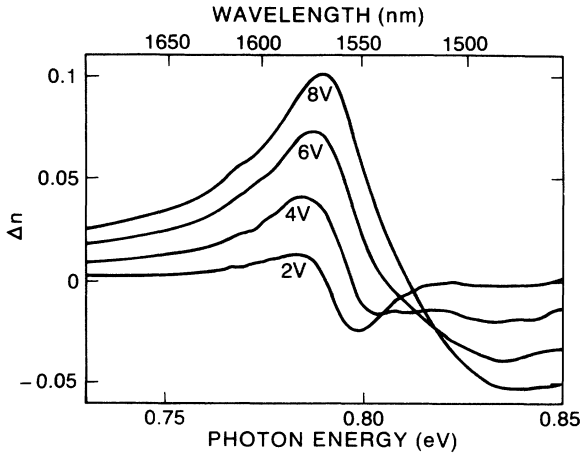

FIG. 10. Differential refractive-index spectra for various biases of sample *B* obtained from Kramers-Kronig transforms of the corresponding normal-incidence absorption spectra. Changes in the refractive index as high as 0.1 can be obtained below the absorption edge.

IV. REFRACTIVE-INDEX SPECTROSCOPY

In Sec. III we have discussed the electron-density-induced changes in the absorption of the quantum well in detail. It is clear that these must be accompanied by refractive-index changes $\Delta n = n(V_{\text{bias}}=0\text{ V}) - n(V_{\text{bias}})$. From Kramers-Kronig considerations, we know that Δn below the band gap is proportional to the spectrally integrated $\Delta\alpha$. Therefore we can expect that the Δn associated with the electron bleaching of the $n_z=1$ transitions, in which $\Delta\alpha$ is always >0, will be much larger than that associated with the quantum confined Stark effect, in which $\Delta\alpha$ is positive in some spectral regions and negative in others.[10] Furthermore, we can expect that the electron-density-induced Δn will be proportional to the lost oscillator strength of the $n_z=1$ transitions. We can predict from the steplike two-dimensional density of states in the QW that no index change occurs as long as the Fermi energy remains below gap. Δn is proportional to $E_F - E_g$ once $E_F > E_g$.

In Fig. 10 we show the Kramers-Kronig transforms of sample *B* for the spectral region around the $n_z=1$ transitions. For the transformation integral the experimental $\Delta\alpha$ over a broad spectral range is used. As expected, we do not observe much index change below gap for 2 V bias, since the Fermi energy has not yet crossed the band gap. As the bias voltage is increased, we find a very large below-gap index change that reaches its maximum of about 0.1 for 8 V just below the band edge.

To confirm this result, we additionally have performed a direct interferometric measurement of Δn in a Mach-Zehnder interferometer. We again use a cw YLF:Nd laser pumped NaCl-F^{2+} color-center laser as a tunable light source. In order to avoid any ambiguity in the interpretation of the measured fringe shift, we restrict ourselves to the spectral region below the absorption edge, where $\Delta\alpha$ is essentially zero, and thus the fringe shift is only given by the change in refractive index. In Fig. 11 we show the directly measured index changes (dots) and compare them with the Kramers-Kronig transform (solid line). The voltage is modulated from 2 to 6 V. The directly measured values are in good agreement with the Kramers-Kronig transform.

The voltage dependence of Δn exhibits the expected behavior. In Fig. 12 we plot this dependence for samples *A* and *B*. The inset again shows the QW region for 1 V bias difference. For sample *B* the measured index change is essentially zero below about 2 V. As the bias is increased further, the index change increases linearly with the applied bias. The solid line in Fig. 12 is a calculation of the electron density in the QW multiplied by the factor $\Delta n / N_e(h\nu)$ as a function of the Fermi energy. The elec-

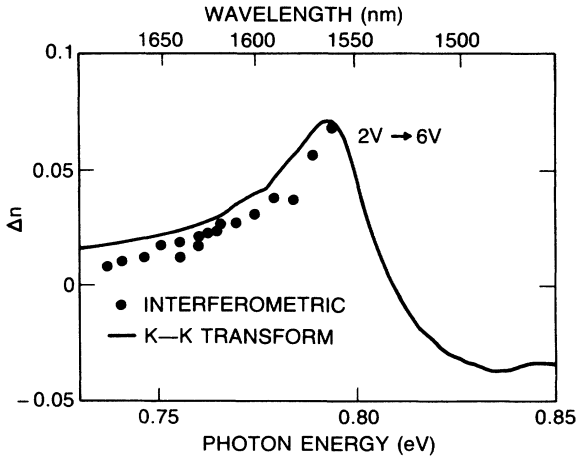

FIG. 11. Differential refractive-index spectrum comparing directly measured Δn values with those obtained from the Kramers-Kronig transform. The bias voltage is modulated from 2 to 6 V.

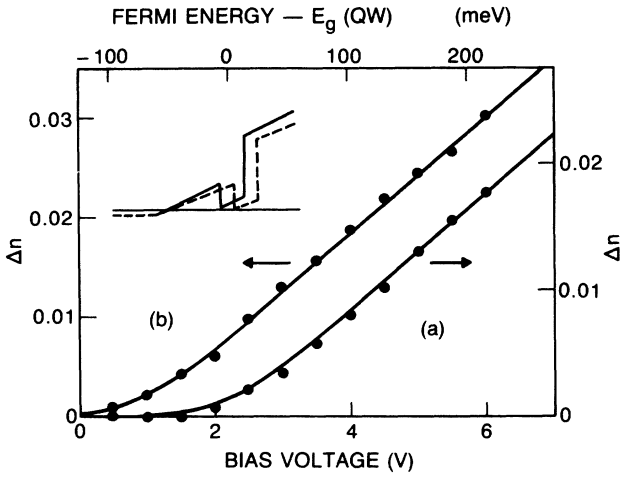

FIG. 12. Change of the refractive index as a function of applied bias voltage. (a) Sample *A* at 1575 nm, and (b) sample *B* at 1590 nm. The dots are the measured values. The solid line is a calculation of the carrier density in the quantum well as a function of the Fermi energy. The agreement between the two shows that the change in refractive index simply reflects the number of electrons in the well.

tron density in a two-dimensional system is simply given by

$$N = -k_B T D_0 \ln\{\exp(E_g - E_F)/[1+\exp(E_g - E_F)]\} \ . \tag{3}$$

D_0 (1.754×10^{13}/eV/cm^2 for In-Ga-As QW's) is the constant density of states in the two-dimensional system. The Fermi energy is then related to the bias. The excellent agreement in Fig. 12 confirms our above-mentioned statement that the index change reflects the electron density in the QW. This is further confirmed by studying sample *B*. As can be seen in the inset, sample *B* is closer to the Fermi energy at zero bias. We thus expect the same behavior shifted to lower biases by about 1 V. Again, direct measurement and calculation are in good agreement.

V. CONCLUSIONS

The influence of thermalized and unthermalized electron-hole populations on the optical properties of semiconductors and semiconductor quantum wells has been subject to extensive studies in recent years. Tunable densities of electron-hole pairs are conveniently introduced by means of optical excitation. Optical excitation, however, does not permit separation of the influences of electrons and holes. We present a novel semiconductor heterostructure that provides a tunable thermalized electron density in multiple quantum wells. From a nearby reservoir the electrons are transferred into the quantum well by applying a bias. Any number of quantum wells can be stacked without inhomogeneities in the density. This may open the door to studies of ultrafast carrier-density-dependent fundamental scattering processes in quantum wells. Furthermore, the large effective blue shift of the quantum-well absorption edge is accompanied by a large change in the refractive index below the gap. This is useful for future light modulator devices; applications to amplitude and, in particular, phase modulation will be reported elsewhere.

[1]IEEE J. Quantum Electron. **QE-22**, 1609–1921 (1986); **QE-24**, 1579–1791 (1988).

[2]H. L. Stormer, R. Dingle, A. C. Gossard, and W. Wiegmann, Solid State Commun. **50**, 735 (1984).

[3]D. S. Chemla, I. Bar-Joseph, C. Klingshirn, D. A. B. Miller, J. M. Kuo, and T. Y. Chang, Appl. Phys. Lett. **50**, 585 (1987).

[4]I. Bar-Joseph, J. M. Kuo, C. Klingshirn, G. Livescu, D. A. B. Miller, T. Y. Chang, and D. S. Chemla, Phys. Rev. Lett. **59**, 1357 (1987).

[5]D. S. Chemla, I. Bar-Joseph, J. M. Kuo, T. Y. Chang, C. Klingshirn, G. Livescu, and D. A. B. Miller, IEEE J. Quantum Electron. **QE-24**, 1664 (1988).

[6]J. H. Abeles, W. K. Chan, A. Kastalsky, J. P. Harbison, L. T. Florez, and R. Bhat, Electron. Lett. **23**, 1302 (1987).

[7]J. M. Kuo, B. Lalevic, and T. Y. Chang, International Electron Device Meeting Technical Digest 460 (1986).

[8]C. Weber, C. Klingshirn, D. S. Chemla, D. A. B. Miller, J. Cunningham, and C. Ell, Phys. Rev. B **38**, 12 748 (1988).

[9]D. A. B. Miller, D. S. Chemla, T. C. Damen, A. C. Gossard, W. Wiegmann, T. H. Wood, and C. A. Burrus, Phys. Rev. Lett. **53**, 2173 (1984).

[10]J. E. Zucker, T. L. Hendrickson, and C. A. Burrus, Appl. Phys. Lett. **52**, 945 (1988).

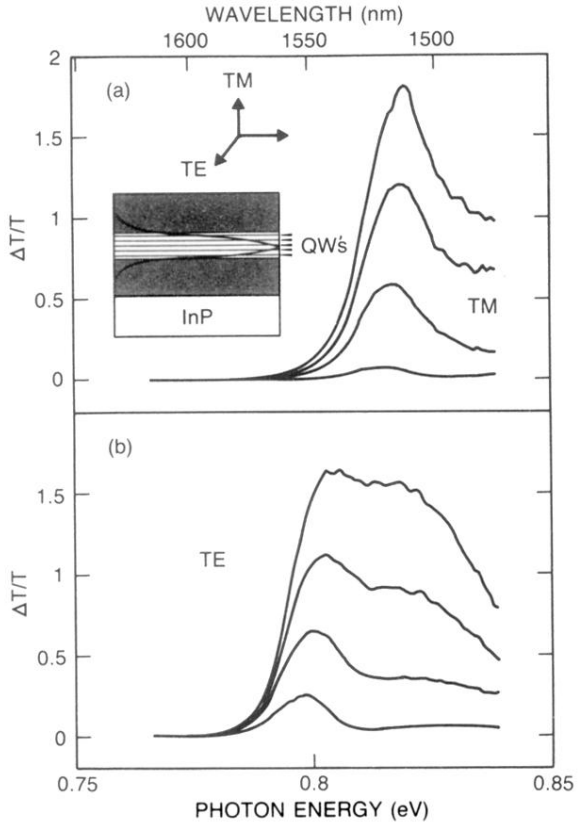

FIG. 8. Waveguide differential transmission spectra for (a) TM and (b) TE polarization of the incoming light. The inset illustrates the geometry. For TM polarization the selection rules forbid the electron–heavy-hole transition and only the light-hole resonance appears. This leads to a maximum light modulation at around 1550 nm in TE polarization, whereas in TM polarization essentially no light modulation is observed at this wavelength.